Aldosterone Exposure Causes Increased Retinal Edema and Severe Retinopathy Following Laser-Induced Retinal Vein Occlusion in Mice

Michael J. Allingham, Nomingerel Tserentsoodol, Peter Saloupis, Priyatham S. Mettu, and Scott W. Cousins

Department of Ophthalmology, Duke University Medical Center, Durham, North Carolina, United States

Correspondence: Michael J. Allingham, Duke Eye Center, Department of Ophthalmology, Duke University Medical Center, 2351 Erwin Road, Durham, NC 27710, USA; mike.allingham@duke.edu.

Submitted: September 29, 2017
Accepted: May 30, 2018

Citation: Allingham MJ, Tserentsoodol N, Saloupis P, Mettu PS, Cousins SW. Aldosterone exposure causes increased retinal edema and severe retinopathy following laser-induced retinal vein occlusion in mice. *Invest Ophthalmol Vis Sci*. 2018;59:3355–3365. https://doi.org/10.1167/iovs.17-23073

Purpose. To determine the effects of aldosterone exposure on retinal edema and retinopathy in a mouse model of retinal vein occlusion (RVO).

Methods. RVO was induced immediately following intravenous injection of Rose bengal (66 mg/kg) using a 532-nm wavelength laser to place three to seven applications at 80 mW and 50-µm spot size directed at the superior retinal vein one disc diameter away from the nerve. Negative control consisted of placing an equal number of laser spots without targeting the vein. Male and female C57BL/6J mice aged 7 to 9 months with confirmed absence of $Crb1^{rd8}$ were used. Aldosterone pellets releasing a daily dose of 0.83 µg/day were implanted subcutaneously 4 weeks prior to RVO. Retinal imaging by optical coherence tomography (OCT) was performed using a Micron IV rodent imaging system. Retinas were analyzed by immunohistochemistry using standard techniques. Retinal imaging and tissue analysis were performed 2, 4, and 7 days following RVO. Comparisons were made using Student's *t*-test, ANOVA, and Pearson's χ^2.

Results. RVO caused retinal edema in the form of cystic spaces and retinal thickening detectable by both OCT and histology. RVO also caused Müller glia (MG) dysfunction manifest as upregulated glial fibrillary acidic protein (GFAP) and altered localization of aquaporin 4 (AQP4) and Kir4.1. Treatment with aldosterone caused a significant increase in retinal edema and more severe retinopathy manifest as retinal whitening and extensive intraretinal hemorrhage. MG dysfunction was more severe and persistent in aldosterone-treated mice. Finally, aldosterone greatly increased the number of infiltrating mononuclear phagocytes following RVO.

Conclusions. Systemic aldosterone exposure causes a more severe RVO phenotype manifest as increased severity and duration of retinal edema and more severe retinopathy. The effects of aldosterone may be mediated by MG dysfunction and increased infiltration of mononuclear phagocytes. This suggests that small increases in aldosterone levels may be a risk factor for severe RVO.

Keywords: retinal vein occlusion, aldosterone, macular edema, retinopathy

Macular edema and progressive ischemic retinopathy are major causes of vision loss in retinal vascular diseases including retinal vein occlusion (RVO). The mainstays of treatment for macular edema include anti-vascular endothelial growth factor agents, corticosteroid therapies, and laser photocoagulation. Thus far, no treatment has proven effective in preventing or reversing ischemic retinopathy. Current treatments have improved patient outcomes, but no therapy is universally effective. Incomplete resolution of edema is seen in 25% to 50% of RVO patients even following aggressive treatment for extended periods.[1,2] Furthermore, some RVO patients experience progressive ischemic retinopathy despite maximum medical therapy.[3] Thus, better understanding of the mechanisms driving the pathobiology of RVO represents an unmet need in order to develop novel therapies.

Aldosterone is a steroid hormone that classically functions via binding to the cytosolic mineralocorticoid receptor (MR) and causing translocation of MR to the nucleus where it mediates transcriptional regulation of numerous gene targets. Aldosterone exposure has been shown to increase disease severity in animal models of both atherosclerosis[4] and vascular endothelial injury.[5] Importantly, clinical trials in humans have also demonstrated better survival and fewer vascular events in patients treated with aldosterone antagonists.[6,7] The retina is a target for the renin–angiotensin–aldosterone system and expresses proteins necessary to both synthesize and respond to aldosterone.[8,9] Aldosterone has been implicated in the pathobiology of vascular diseases affecting the retina. For example, an experimental model of retinal neovascularization is made more severe by MR activation and is ameliorated by its blockade.[9] Intravitreal injection of aldosterone caused increased retinal thickness associated with altered expression and distribution of Müller glia (MG), aquaporin 4 (AQP4), and Kir4.1 in rats,[8] suggesting effects on retinal fluid homeostasis. However, the effect of MR activation in the context of pathologic retinal edema has not yet been addressed. RVO

manifests both retinopathy and macular edema, both of which may be affected by aldosterone. We hypothesized that aldosterone would cause more severe retinal edema and retinopathy and utilized low-dose, systemic aldosterone treatment to determine the impact of MR activation in the RVO model. To explore this hypothesis, we have used a modified RVO protocol in the mouse.

Methods

Animals

All animal experiments adhered to the ARVO Statement for the Use of Animals in Ophthalmic and Vision Research following institutionally approved protocols. We used both male and female C57BL/6J mice aged 7 to 9 months with confirmed absence of $Crb1^{rd8}$ (Jackson Labs, Bar Harbor, ME, USA). Mice were housed in groups of two to five in temperature- and humidity-controlled conditions under a 12-hour light and dark cycle. Mice were fed standard chow and had free access to water. At the end of a given experiment, mice were killed by carbon dioxide inhalation followed by bilateral thoracotomy.

In total 40 mice were used for in vivo imaging studies with three groups of 3 or 4 mice receiving sham or aldosterone treatment (20 mice), plus controls and sham-lasered eyes (20 mice). For immunohistochemistry (IHC), five to seven eyes per condition were analyzed. For flat-mount ionized calcium-binding adaptor molecule 1 (Iba1) staining, 10 eyes per condition were analyzed. For Western blots, three retinas per condition were analyzed. Experiments comparing standard RVO and RVO with aldosterone were repeated in three cohorts of control and aldosterone-treated mice using male and female mice. Sham laser or RVO was performed in both eyes, but each eye was utilized for different experimental purposes.

Aldosterone pellets were purchased from Innovative Research of America (Sarasota, FL, USA). Each pellet contained 0.05 mg/pellet of aldosterone and released a daily dose of 0.83 μg/day. Pellets were implanted in the subcutaneous tissue between the shoulder blades 4 weeks prior to RVO and were left in place for the duration of subsequent study.

Laser-Induced Retinal Vein Occlusion

Pupils were dilated using tropicamide 0.5%/phenylephrine 2.5% drops. Mice were anesthetized using intraperitoneal injection of ketamine and xylazine (100 and 5 mg/kg); RVO was induced using an Iris Medical Oculight GLX (Mountain View, CA, USA) 532-nm wavelength laser to place three to seven applications at 80 mW and 50-μm spot size directed at the superior retinal vein located approximately one disc diameter away from the optic nerve. A coverslip was applied to the cornea and laser was applied immediately following intravenous injection of Rose bengal (66 mg/kg) via the tail vein. This concentration of Rose bengal was selected because it produced more reliable vein occlusion with fewer laser applications. Negative control (sham) consisted of placing an equal number of laser spots without targeting the retinal vein. All procedures were performed using general anesthesia to maintain comfort.

Immunohistochemistry

Enucleated eyes were postfixed for 4 hours in 4% paraformaldehyde (PFA), then overnight in 1% PFA. Fixed retinas were incubated in 30% sucrose in PBS for 1 hour, then embedded in optimal cutting temperature (OCT) medium (Sakura, Torrance, CA, USA), and snap-frozen in liquid nitrogen. Serial 20-μm sections were blocked for 1 hour with 10% normal donkey serum (Jackson Immunoresearch, West Grove, PA, USA) in 0.01% Triton X-100, then overnight with primary antibodies: rabbit anti-aquaporin 4 (Sigma-Aldrich Corp., St. Louis, MO, USA), rabbit anti-Kir4.1 (Alomone Labs, Jerusalem, Israel), and goat anti-glial fibrillary acidic protein (Abcam, Cambridge, MA, USA). Immunostaining was visualized using Alexa 568– and 647–conjugated secondary antibodies (Thermo Fisher Scientific, Waltham, MA, USA). Slides were mounted with Fluoromount G (Electron Microscopy Sciences, Hatfield, PA, USA) and coverslipped. All imaging was performed on Nikon C2 and A1 confocal laser scanning microscopes with NIS-Elements AR 50.0 software (Nikon, Melville, NY, USA). To ensure that the affected region of the retina was analyzed by IHC, we occluded a superior retinal vein, and the superior aspect of the globe was marked using a suture during enucleation and subsequent tissue processing. During dissection of the eyes, the occluded vein and region of interest was confirmed and identified under a dissecting microscope.

Quantification of AQP4, Kir4.1, and GFAP by Immunofluorescence Microscopy

Fluorescence intensity of GFAP, AQP4, and Kir4.1 staining in specific retinal layers was quantified using Adobe Photoshop CS4 software (San Jose, CA, USA). The nerve fiber layer (NFL), inner plexiform layer (IPL), inner nuclear layer (INL), outer plexiform layer (OPL), and outer nuclear layer (ONL) were manually segmented using nuclear staining (Hoechst, 1:10,000 dilution; Thermo Fisher Scientific) to identify and delineate the borders of each layer. The mean intensity was determined using the Histogram function. The results were averaged from the five to seven images from the same group and then expressed as mean ± standard deviation. NT obtained confocal images, and these were evaluated and quantified in masked fashion by MJA.

Western Blotting

Western blotting was performed as previously described.[10] Briefly, proteins were extracted from whole retinas by homogenization of retinal tissue in 160 μL radioimmunoprecipitation assay buffer (RIPA) lysis buffer with protease inhibitors (Roche Molecular Biochemicals, Indianapolis, IN, USA). Total protein concentration was measured using the Pierce BCA Protein Assay Kit (Thermo Fisher Scientific) and samples were diluted with SDS/PAGE sample buffer to achieve 1 mg/mL concentrations and stored in aliquots at –80°C. Protein (20 μg) was loaded and run on 4% to 15% Tris/glycine mini-precast gels (Bio-Rad, Hercules, CA, USA) at 100 V for 1 hour. Proteins were transferred onto polyvinylidene difluoride (PVDF) membranes (Bio-Rad). Primary antibodies were used as follows: AQP4 1:1000; Kir4.1: 1:400, and GFAP 1:2000. Protein levels were normalized to mouse anti-β-actin, which was used as a loading control (1:500; Santa Cruz Biotechnology, Inc., Dallas, TX, USA). Secondary antibodies were horseradish peroxidase–conjugated donkey anti-rabbit, donkey anti-goat, and donkey anti-mouse used at 1:3000 dilution (Jackson Immunoresearch). West Pico PLUS Chemiluminescent Substrate was used (Thermo Fisher Scientific), and blots were imaged using the ChemiDoc Touch system (Bio-Rad). Intensity of immunoreactive bands was quantified by Adobe Photoshop CS4. Protein levels were then normalized to control eyes to generate a fold change in protein expression.

Quantification of Iba1-Positive Cells Following RVO

Following RVO, eyes were harvested and postfixed as above. Fixed retinas were carefully removed from underlying retinal

Investigative Ophthalmology & Visual Science

pigment epithelium and blocked in 0.01% Triton X-100 and 10% normal donkey serum (Jackson Immunoresearch). Mononuclear phagocytes were labeled using rabbit anti-Iba1 (Wako, Osaka, Japan), and cell nuclei were counterstained with Hoechst (Thermo Fisher Scientific). Retinal whole mounts were then placed on glass slides and mounted using Fluoromount G (Electron Microscopy Sciences) and coverslipped. Whole retinas were imaged at ×10 magnification using a motorized translational stage (Prior ProScan III; Prior Scientific, Rockland, MA, USA). For image analysis, three regions of retina in the quadrant affected by RVO were imaged by confocal microscope, and full-thickness Z-stacks were generated at ×20 magnification. Cells in these fields were counted if the Iba1-positive staining was associated with a nucleus. Three regions of retina opposite the quadrant affected by RVO were analyzed in identical fashion. Untreated controls and sham laser controls were analyzed similarly. All imaging was performed on Nikon C2 and A1 confocal laser scanning microscopes with NIS-Elements AR 50.0 software (Nikon).

Mouse In Vivo Retinal Imaging

Mice were anesthetized as described above and fundus photos, optical coherence tomography (OCT) images, and fluorescein angiograms (FA) were obtained using a Micron IV rodent imaging system (Phoenix Research Labs, Pleasanton, CA, USA). For FA, 0.03 mL of 10 mg/mL sodium fluorescein (Akorn, Lake Forest, IL, USA) was injected intraperitoneally and mice were imaged using standard excitation/emission filters included with the Micron IV instrument. Following RVO, mice were imaged by OCT and fundus camera on days 2, 4, and 7. The presence of any retinal hemorrhage was noted at each time point. Presence of intraretinal fluid was counted if there were greater than two visible cysts in at least two different B-scans. Volume scans of edematous retina located outside the area of laser application were acquired, and the B-scan containing maximal retinal thickness was used in comparisons of maximal retinal thickness between groups. Additionally, the average retinal thickness across an entire B-scan was calculated for a scan located in the center of the affected region of retina. This was performed by using the Insight software package (Phoenix Research Labs) to segment the region between the inner limiting membrane and the base of the retinal pigment epithelium. The raw data containing the thickness for 1024 individual A-scans were exported to Excel (Microsoft, Redmond, WA, USA), and an average thickness was then calculated. OCT retinal thickness measurements and presence of retinal hemorrhage and intraretinal fluid were evaluated in a masked fashion by PSM and MJA, who are both expert retinal clinicians and laboratory scientists experienced in the interpretation of retinal imaging. Disagreements were adjudicated by SWC.

Statistical Analysis

The mean and standard deviation of each group were calculated, and Student's *t*-test was used to compare two groups. For binary outcomes such as presence of intraretinal hemorrhage, Pearson's χ^2 testing was performed. For comparisons of means across multiple groups ANOVA testing was used. Statistical calculations were performed using JMP13 (SAS Institute, Cary, NC, USA). Results at $P < 0.05$ were considered statistically significant.

Results

Retinal Vein Occlusion Causes Retinal Edema

Several groups have used laser induced vein occlusion in mouse and rat to characterize the response of various retinal cell types following vein occlusion.[11–17] Most have occluded half or all retinal veins, which leads to extensive ischemia and eventual retinal neovascularization. We altered this approach by occluding only a single vein and examining the tissue in the peripheral retina that is drained by the occluded vein. To determine the natural history of our RVO protocol in mice, we obtained fundus photos and OCT on days 2, 4, and 7 following RVO. Representative color fundus and OCT images from three different mice are shown in Figure 1. Sham laser did not cause any retinal edema at day 2 (Fig. 1) or at subsequent time points (data not shown). Two days following RVO, fluorescein angiography (FA) showed occlusion of a single retinal vein and mild leakage. Fundus examination showed intraretinal hemorrhage in some eyes and OCT showed retinal thickening with intraretinal cysts located predominantly in the inner nuclear and plexiform layers. The vast majority of eyes showed some cystic intraretinal fluid at day 2 and this resolved in all cases by day 7. Intraretinal hemorrhage was noted in 25% of eyes and this also resolved by day 7. Reperfusion of the occluded vein typically takes place between day 2 and 4.

Low-Dose Systemic Aldosterone Causes Severe Edema and Retinopathy Following RVO

To determine the effects of aldosterone on retinal edema, mice were treated with bioerodible aldosterone pellets 4 weeks prior to RVO. Studies of the effects of aldosterone in other disease models have used doses ranging from 0.55 to 2000 μg/day.[9,18,19] We selected a low dose of 0.83 μg/day because subclinical, chronic MR activation is suggested to be present in numerous other vascular disease states,[20] many of which share risk factors with RVO. Aldosterone treatment prior to RVO caused more severe edema and retinopathy (Fig. 2A). Fluorescein angiography shows occlusion of a single vein but suggests capillary nonperfusion and shows more intense leakage. Fundus imaging showed retinal whitening and multifocal hemorrhage, which were widespread and were not seen in the standard RVO model. OCT showed more severe retinal thickening and cystic intraretinal fluid as well as increased hyperreflectivity of the inner retinal layers, suggesting ischemia. Quantification of maximal retinal thickness as well as average retinal thickness within a B-scan across the center of the affected region on OCT at days 2, 4, and 7 showed that retinal edema was both more severe and more persistent in aldosterone-treated mice (Fig. 2B). Differences in maximal retinal thickness were statistically significant at days 2 and 4 ($P = 0.03$ and 0.0001, respectively), as were differences in average retinal thickness ($P = 0.04$ and 0.009, respectively). To further quantify the effects of aldosterone, the proportion of eyes manifesting intraretinal fluid and hemorrhage was determined (Fig. 2C). In aldosterone-treated mice, the proportion of eyes manifesting cystic intraretinal fluid was higher at days 4 and 7 ($P = 0.001$ and $P = 0.02$, respectively). Interestingly, aldosterone-treated mice manifested progressive retinopathy following RVO, which appeared as an increasing proportion of eyes with intraretinal hemorrhage. By contrast, the proportion of eyes manifesting intraretinal hemorrhage fell rapidly in controls. This difference was statistically significant at days 4 and 7 ($P = 0.04$ and $P = 0.002$, respectively).

RVO and Aldosterone Cause Müller Glial Injury

MG dysfunction contributes to the pathogenesis of retinal edema, and RVO has been shown to impact the expression and distribution of glial fibrillary acidic protein (GFAP) as well as AQP4 and Kir4.1.[11] We used GFAP as a marker of MG injury. To determine the effects of RVO on MG, IHC was performed to further characterize retinal morphologic changes and the MG

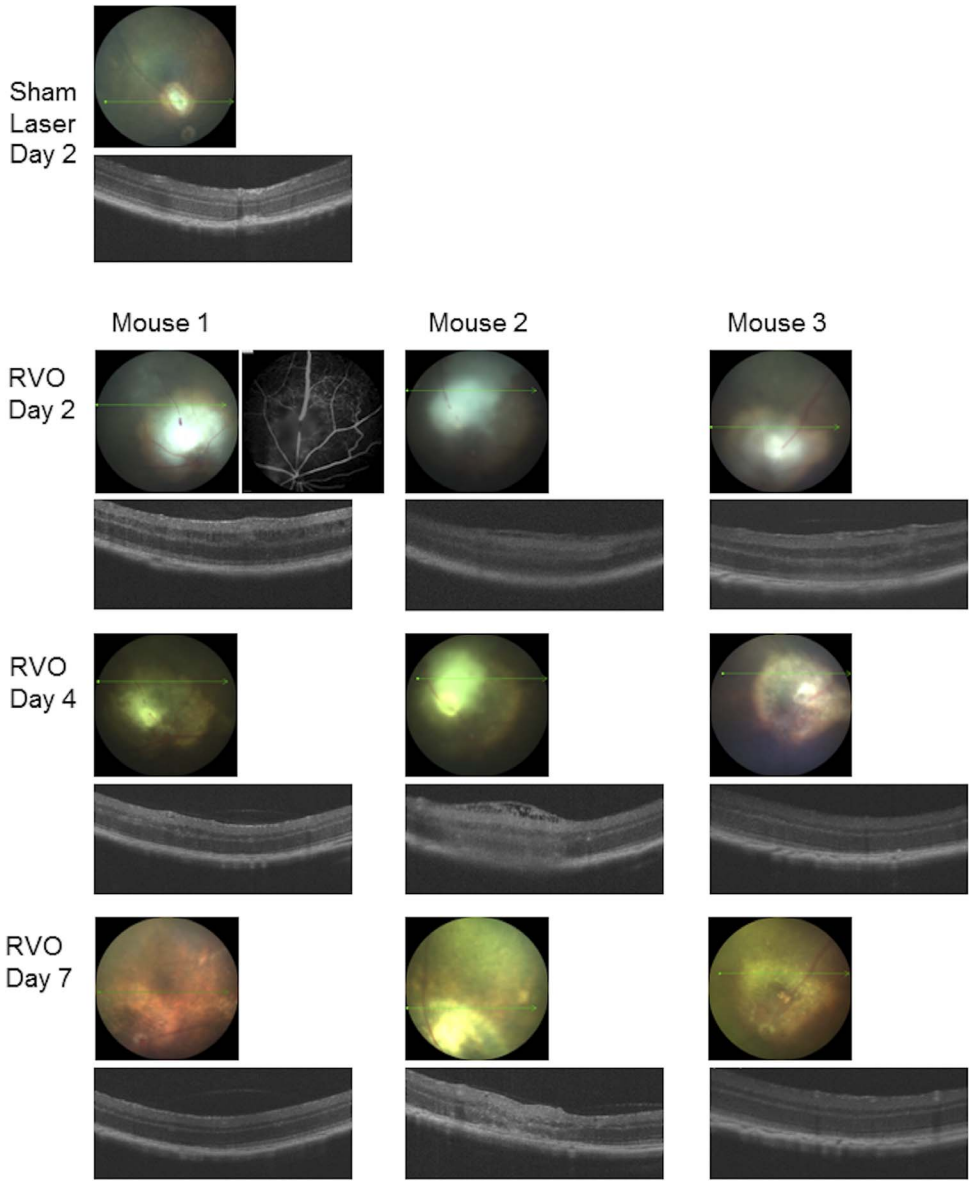

Figure 1. Retinal vein occlusion causes retinal edema. The *upper* parts of the figure show fundus photo and OCT image 2 days after sham laser. There is no edema or hemorrhage. Three representative examples of fundus imaging and OCT following standard RVO are shown. For mouse 1, an FA from day 2 is also included. Two days following RVO, the vein remains occluded and there is mild retinal edema with small cysts visible in the inner nuclear layer. FA shows leakage around the occluded vein. By day 4, there is reduced intraretinal fluid in most cases and by day 7, fluid has resolved. In some cases there is disorganization of inner retinal layers as seen in mouse 2 ($n = 8$–10 eyes per condition).

responses to RVO. We first investigated GFAP staining as a marker of MG injury. Figure 3 shows GFAP staining in control, sham, and eyes analyzed 2, 4, and 7 days following RVO. Immunofluorescence intensity was quantified in the NFL, IPL, INL, OPL, and ONL, and total retinal GFAP expression was quantified by Western blot at each time point. Sham laser did not change GFAP staining or protein levels. Interestingly, GFAP staining was increased in the NFL in aldosterone-treated eyes compared to controls ($P = 0.002$), suggesting that aldosterone exposure alone causes MG injury. Following RVO, statistically significant increases in GFAP staining were seen in all retinal layers at all time points compared to control ($P < 0.05$ for all), suggesting that RVO with or without aldosterone causes significant MG injury. In order to compare the effects of aldosterone exposure on the distribution of GFAP within MG, staining levels in retinal layers were compared between control and aldosterone-treated mice at each time point. In aldosterone-treated eyes receiving RVO, modest but statistically significant increases in GFAP staining were seen in the NFL and ONL at day 2 ($P = 0.02$ for both), ONL at day 4 ($P = 0.04$), and ONL and OPL ($P = 0.01$ and 0.03, respectively) at day 7 compared to standard RVO. Morphologically, intraretinal cysts were noted primarily in the INL and within the plexiform layers to a lesser extent, which corresponds to their distribution as seen by OCT. In order to quantify GFAP protein expression, Western blot was performed. This showed similar increases in total GFAP protein expression between control and aldosterone-exposed mice, suggesting that GFAP distribution within MG is affected to a greater extent than total GFAP expression. Taken together, these data suggest that some preexisting MG injury is present due to aldosterone exposure

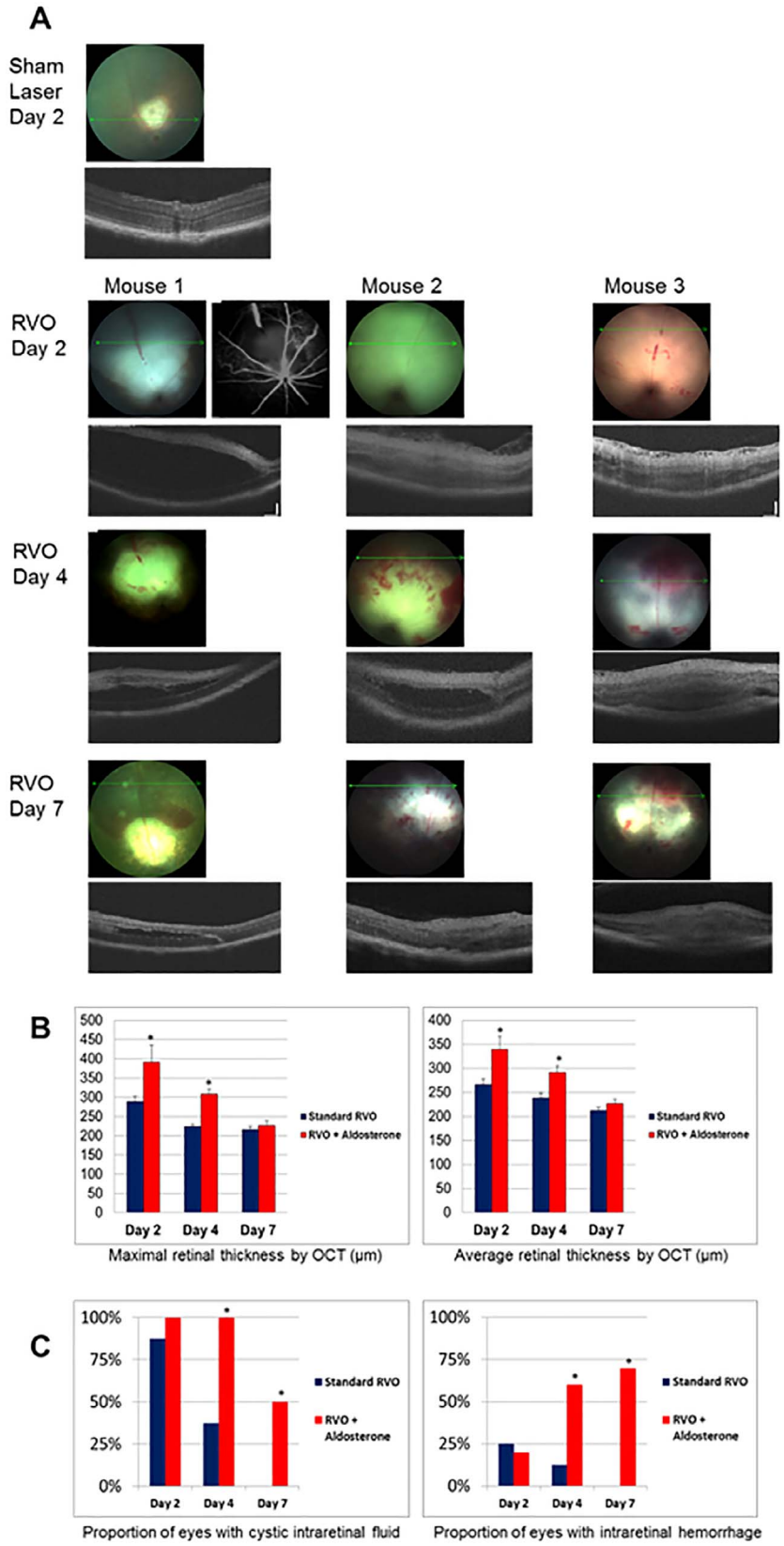

Figure 2. Low-dose systemic aldosterone causes severe edema and retinopathy following RVO. (**A**) Sample images 2 days following sham laser in aldosterone-exposed mouse are shown. There is no hemorrhage or edema. Three representative fundus and OCT images on days 2, 4, and 7 following RVO are shown. An FA image from day 2 is included for mouse 1 and shows capillary nonperfusion and extensive leakage. Fundus images demonstrate early diffuse retinal whitening while OCT shows inner retinal hyperreflectivity and major retinal thickening on day 2, diffuse severe hemorrhage and persistent cystic edema on day 4, and decreasing but persistent hemorrhage and retinal thickening on day 7 ($n = 8$–10 eyes per condition). (**B**) Maximal retinal thickness (*left*) and average retinal thickness (*right*) were quantified at each time point in mice receiving RVO or

aldosterone plus RVO ($n = 8$–10 eyes per condition). Maximum and average retinal thickness are greater in aldosterone-treated mice on days 2 and 4 ($P = 0.03$ and 0.0001 for maximum thickness on day 2 and 4, respectively, $P = 0.04$ and 0.009 for average thickness on day 2 and 4, respectively). (**C**) The proportion of eyes manifesting cystic intraretinal fluid (*left*) and intraretinal hemorrhage (*right*) was quantified ($n = 8$–10 eyes per condition). Aldosterone caused more frequent and persistent fluid compared to control ($P = 0.001$ and $P = 0.02$, for days 4 and 7, respectively). Aldosterone caused increased intraretinal hemorrhage on days 4 and 7 ($P = 0.04$ and $P = 0.002$, respectively). *Asterisk* indicates $P < 0.05$.

and that this injury is more persistent following RVO in aldosterone-exposed mice.

Aldosterone Causes More Severe MG Fluid Transport Dysfunction Following RVO

Because aldosterone treatment caused more severe retinal edema after RVO as measured by OCT, we wished to determine whether more severe MG fluid transport dysfunction contributed to this observation. AQP4 and Kir4.1 are water and potassium channels critical for MG-mediated fluid transport[21,22] and were used as markers of MG fluid transport function. We first analyzed AQP4 staining and protein expression as described for GFAP in order to determine the impact of aldosterone on RVO-induced MG fluid transport function (Fig. 4). Sham laser did not impact AQP4 staining. Interestingly, AQP4 became diffusely redistributed and showed increased staining in the ONL, OPL, INL, and IPL in control and sham-lasered aldosterone-exposed mice ($P < 0.005$ for all). We next compared AQP4 staining in retinal layers following RVO in control and aldosterone-exposed mice. At day 2, AQP4 staining was more intense in the ONL and OPL in aldosterone-exposed mice ($P = 0.0001$ and 0.001, respectively) and was decreased in NFL ($P = 0.04$). At day 4, AQP4 staining was increased in all

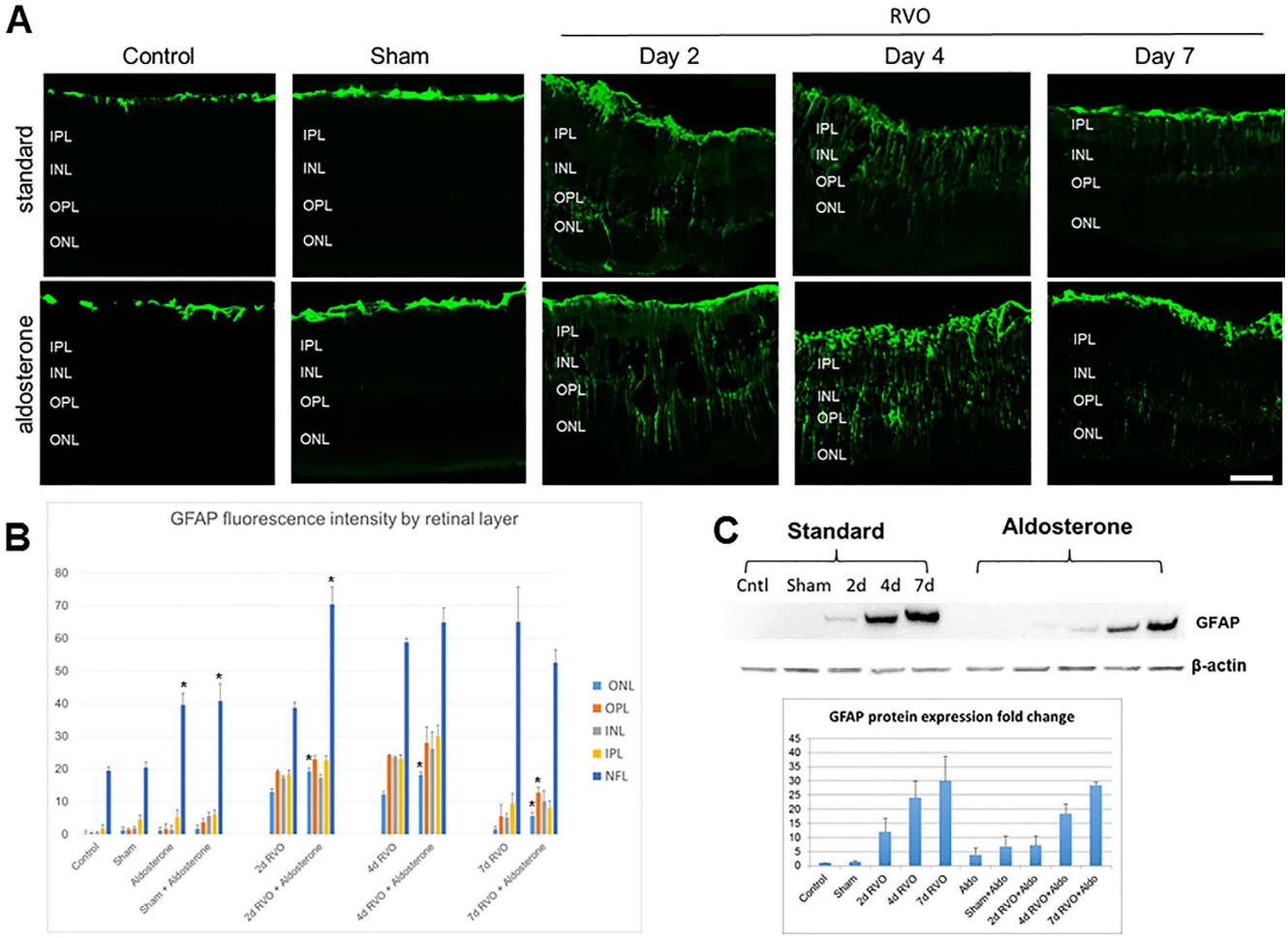

Figure 3. RVO and aldosterone cause Müller glial injury. (**A**) GFAP staining in control, sham laser, and 2, 4, and 7 days following RVO in control mice (*upper*) or aldosterone-exposed mice (*lower*). Sham laser did not significantly impact staining or retinal morphology outside the immediate region of the laser application. (**B**) Quantification of fluorescence intensity in NFL, IPL, INL, OPL, and ONL in control, sham, and RVO eyes with and without aldosterone exposure (arbitrary units). GFAP staining was increased in the NFL in aldosterone-treated eyes compared to controls ($P = 0.002$ for control and sham), suggesting that aldosterone exposure alone causes MG injury. Following RVO, statistically significant increases in GFAP staining were seen in all retinal layers at all time points compared to control ($P < 0.05$ for all), suggesting that RVO with or without aldosterone causes significant MG injury. In aldosterone-treated eyes receiving RVO, statistically significant increases in GFAP staining compared to corresponding control were seen in the NFL and ONL at day 2 ($P = 0.02$ for both), ONL at day 4 ($P = 0.04$), and ONL and OPL ($P = 0.01$ and 0.03, respectively) at day 7 compared to standard RVO. (**C**) Representative Western blot and quantification showing changes in GFAP total protein in isolated retina under various conditions. In both control and aldosterone-exposed mice, GFAP expression rose steadily following RVO. Differences between control and aldosterone-treated mice were not significant. ($n = 5$–7 eyes per condition for IHC and 3 retinas per condition for Western blot; *scale bar*: 50 μm; *asterisk* indicates $P < 0.05$).

Investigative Ophthalmology & Visual Science

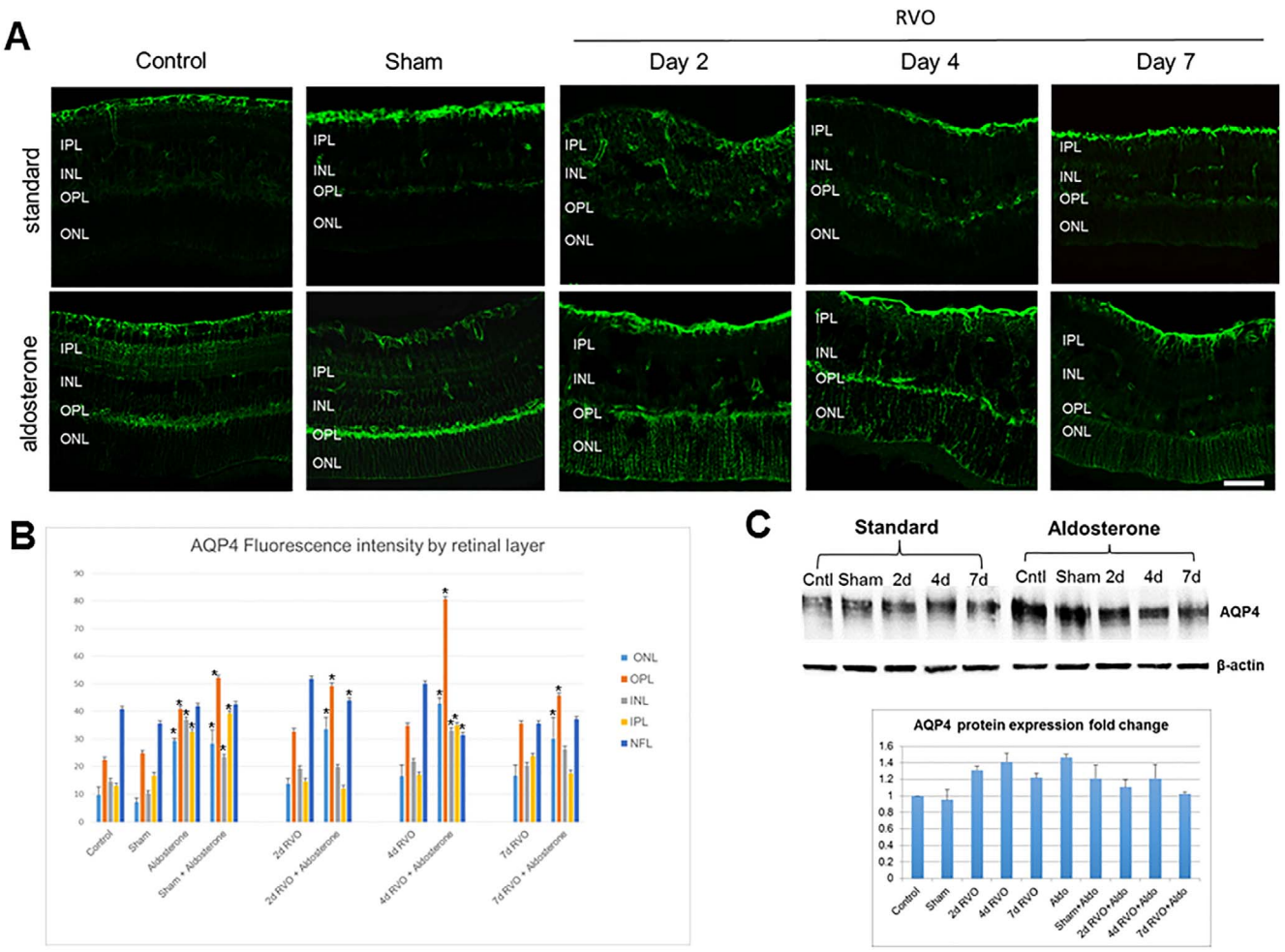

Figure 4. Effects of aldosterone on AQP4 localization and protein expression in control and RVO eyes. (**A**) AQP4 staining in control, sham laser, and 2, 4, and 7 days following RVO in control mice (*upper*) or aldosterone-exposed mice (*lower*). Sham laser did not significantly impact staining or retinal morphology outside the immediate region of the laser application. (**B**) Quantification of fluorescence intensity in NFL, IPL, INL, OPL, and ONL in control, sham, and RVO eyes with and without aldosterone exposure (arbitrary units). Aldosterone exposure caused AQP4 to become diffusely redistributed with increased staining in the ONL, OPL, INL, and IPL in control and sham-lasered mice ($P < 0.005$ for all). At day 2 after RVO, AQP4 staining was more intense in the ONL and OPL in aldosterone-exposed mice ($P = 0.0001$ and 0.001, respectively) and was decreased in NFL ($P = 0.04$). At day 4, AQP4 staining was increased in all layers except NFL where it was decreased ($P < 0.0001$ for all). At day 7, staining was increased in the ONL and OPL of aldosterone-exposed mice ($P = 0.001$ and 0.003, respectively). (**C**) Representative Western blot and quantification showing changes in AQP4 total protein in isolated retina under various conditions. Analysis of AQP4 protein expression did not show statistically significant changes in AQP4 protein expression on average ($n = 5$–7 eyes per condition for IHC and 3 retinas per condition for Western blot; *scale bar*: 50 μm; *asterisk* indicates $P < 0.05$).

layers except NFL, where it was decreased ($P < 0.0001$ for all). At day 7, staining was increased in the ONL and OPL ($P = 0.001$ and 0.003, respectively). Analysis of AQP4 protein expression did not show statistically significant changes in AQP4 protein expression on average. This suggests that AQP4 is redistributed more diffusely across MG due to aldosterone exposure and that this persists following RVO. These changes take place without major effects on total protein expression.

We next performed a similar analysis of Kir4.1 staining and protein expression (Fig. 5). Again, sham laser did not change Kir4.1 staining. Of note, we found that Kir4.1 also became more diffusely redistributed and showed increased staining in the OPL, INL, and IPL in both control and sham-lasered eyes in aldosterone-exposed mice ($P < 0.005$ for all). Following RVO, Kir4.1 staining was decreased in the RNFL at all time points in both control and aldosterone-exposed mice ($P < 0.0001$ for all). The increased outer retinal staining seen in aldosterone-exposed mice was lost following RVO. Analysis of Kir4.1 protein expression showed a rapid decrease in total Kir4.1 expression in both control and aldosterone-exposed mice. Differences between control and aldosterone-exposed mice were significant at days 2 and 4 ($P < 0.0001$, $P = 0.04$, respectively). These results suggest that aldosterone exposure causes Kir4.1 redistribution prior to RVO and that loss of Kir4.1 expression is more pronounced following RVO in aldosterone-exposed mice.

Aldosterone Increases Mononuclear Phagocyte Recruitment Following RVO

Aldosterone treatment has been associated with increased recruitment of mononuclear phagocytes in models of retinal neovascularization.[9] We wished to explore the hypothesis that aldosterone treatment increases mononuclear phagocyte recruitment following RVO. We performed Iba1 staining to label mononuclear phagocytes in retinal flat mounts in eyes 7 days after sham laser, aldosterone plus sham laser, RVO, and aldosterone plus RVO (Fig. 6A). Day 7 was selected based on

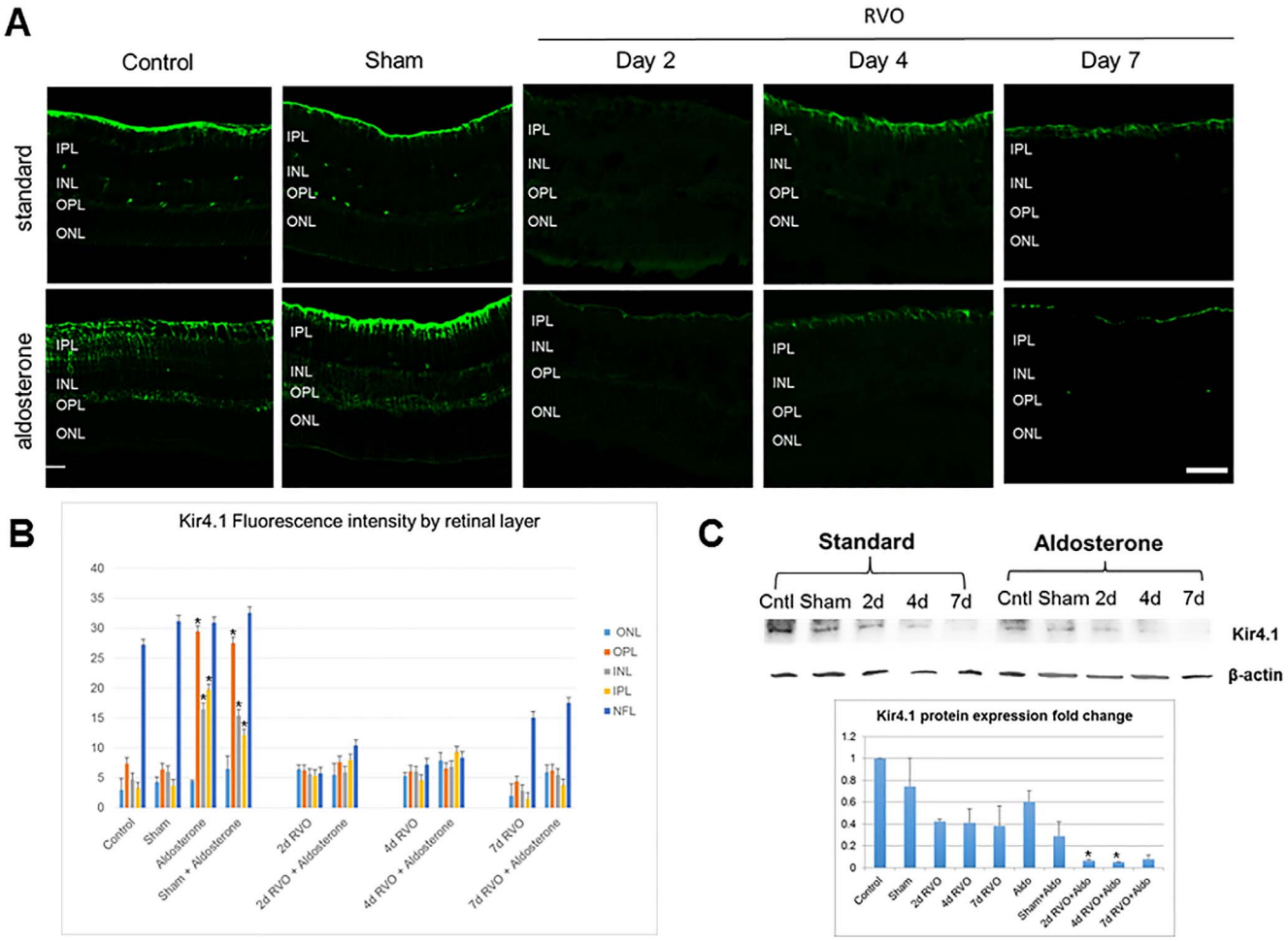

Figure 5. Effects of aldosterone on Kir4.1 localization and protein expression in control and RVO eyes. (**A**) Kir4.1 staining in control, sham laser, and 2, 4, and 7 days following RVO in control mice (*upper*) or aldosterone-exposed mice (*lower*). Sham laser did not significantly impact staining or retinal morphology outside the immediate region of the laser application. (**B**) Quantification of fluorescence intensity in NFL, IPL, INL, OPL, and ONL in control, sham, and RVO eyes with and without aldosterone exposure (arbitrary units). Kir4.1 showed increased staining in the OPL, INL, and IPL in both control and sham-lasered eyes in aldosterone-exposed mice ($P < 0.005$ for all). Following RVO, Kir4.1 staining was decreased in the RNFL at all time points in both control and aldosterone-exposed mice ($P < 0.0001$ for all). The increased outer retinal staining seen in aldosterone-exposed mice was lost following RVO. (**C**) Representative Western blot and quantification showing changes in AQP4 total protein in isolated retina under various conditions. Analysis of Kir4.1 protein expression showed a rapid decrease in total Kir4.1 expression in both control and aldosterone-exposed mice. Differences between control and aldosterone-exposed mice were significant at days 2 and 4 ($P < 0.0001$, $P = 0.04$, respectively) ($n =$ 5–7 eyes per condition for IHC and 3 retinas per condition for Western blot; *scale bar*: 50 µm, *asterisk* indicates $P < 0.05$).

the previously reported finding by Ebneter and colleagues[13] showing maximal mononuclear phagocyte recruitment at day 7 after RVO. There was an apparent increase in density of Iba1-positive cells in areas affected by vein occlusion but not in sham laser eyes or areas distant from vein occlusion. Mononuclear phagocytes in the RVO-affected region displayed a more rounded morphology compared to the dendritic morphology seen in control and unaffected regions. We next quantified Iba1-positive cells in the RVO-affected quadrant and in an unaffected quadrant of the flat mount (Fig. 6B). Mononuclear phagocytes were not increased in eyes that underwent sham laser or aldosterone treatment plus sham laser. We found that the number of Iba1-positive cells was significantly increased in the region affected by RVO, but not in other areas of the retina ($P < 0.001$). Interestingly, the number of mononuclear phagocytes in RVO-affected areas was much higher in aldosterone-treated mice compared to RVO alone as well as controls, and this was statistically significant ($P <$ 0.0001).

Discussion

Retinal vein occlusion in the mouse reproduces important features of RVO in humans including cystic intraretinal fluid accumulation and intraretinal hemorrhage. Treatment of mouse RVO with anti-VEGF ameliorates edema and leakage as seen in humans.[14] This suggests that mouse RVO is a useful model for the study of pathobiology and testing of other potential treatments for RVO or macular edema. We have found that systemic aldosterone treatment significantly increases both retinal edema and the severity of retinopathy following RVO. The findings of retinal whitening and diffuse hemorrhage on fundus exam, capillary nonperfusion on FA, and inner retinal hyperreflectivity by OCT suggest that aldosterone may induce an ischemic RVO phenotype. This hypothesis as well as the precise mechanism by which aldosterone induces this phenotype is deserving of future study.

Aldosterone may worsen RVO phenotype by at least two potential pathways. First, aldosterone treatment may worsen MG dysfunction in RVO. MG regulate retinal fluid homeosta-

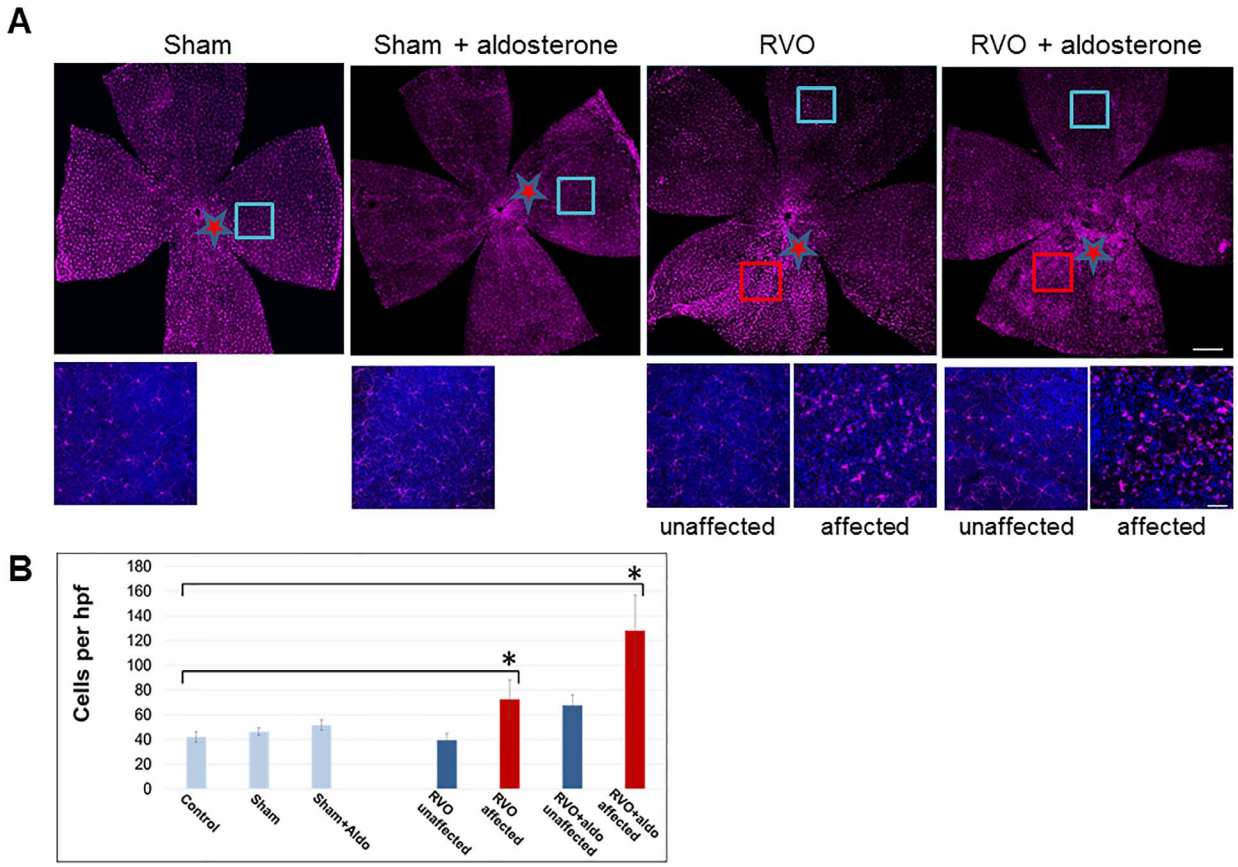

Figure 6. Aldosterone increases mononuclear phagocyte recruitment following RVO. (**A**) Iba1 staining for mononuclear phagocytes in retinal flat mounts in eyes 7 days after sham laser, aldosterone plus sham laser, RVO, and aldosterone plus RVO. *Top* parts of figure show Iba1 staining in flat mounts, with *star* showing site of laser application and *blue* and *red squares* showing region imaged in *lower* figure parts. *Lower* parts of figure show high-powered image of Iba1-positive cells in the corresponding region in the flat mount. RVO eyes have one high-powered field from the RVO-affected region (*red*) and from an unaffected region (*blue*). Sham laser eyes have a single high-power view showing Iba1-positive cell morphology. In flat mounts, there was an apparent increase in density of Iba1-positive cells in areas affected by vein occlusion but not in sham laser eyes or areas distant from vein occlusion. Mononuclear phagocytes in the RVO-affected region displayed a more rounded morphology compared to the dendritic morphology seen in control and unaffected regions (*Scale bars*: 200 μm for *top* and 50 μm for *bottom*). (**B**) Quantification of Iba1-positive cells demonstrates statistically significant increase in mononuclear phagocyte infiltration in RVO-affected regions compared to all controls and unaffected regions ($P < 0.0001$). Aldosterone caused significant increase in infiltration of mononuclear phagocytes compared to all controls and RVO alone ($P < 0.0001$ for all) ($n = 10$ flat mounts per condition; *asterisk* indicates $P < 0.05$).

sis,[8,21] vascular permeability,[23] and retinal endothelial proliferation.[24] Thus, aldosterone-induced MG dysfunction could have numerous impacts on RVO phenotype. We have found that aldosterone treatment altered distribution of GFAP, AQP4, and Kir4.1 in control eyes that did not receive RVO, suggesting a direct effect of systemic aldosterone on MG (Figs. 3–5). Importantly, aldosterone also caused more widespread and prolonged AQP4 redistribution as well as more pronounced downregulation of Kir4.1 after RVO. Because MG pump function depends on specific expression and colocalization of AQP4 and Kir4.1,[21,22] the redistribution of AQP4 and Kir4.1 and loss of Kir4.1 expression may contribute to intraretinal fluid accumulation seen by OCT and cystic spaces seen by IHC. We hypothesize that aldosterone interferes with MG pump function by mediating redistribution of AQP4 and Kir4.1, as well as more pronounced loss of Kir4.1 expression, and possibly by other undiscovered mechanisms leading to more severe retinal edema. Future studies will be directed toward delineating the specific pathways by which aldosterone-mediated MG dysfunction drives severe RVO.

A second mechanism by which aldosterone may worsen RVO is by enhancing the recruitment of mononuclear phagocytes. Aldosterone-treated mice had greatly increased numbers of mononuclear phagocytes in RVO-affected regions of the retina. However, we did not see an increase in the number of mononuclear phagocytes present in aldosterone-treated mice that underwent only sham laser. This suggests that the effects of aldosterone at the tested dose and duration depend on an inciting vascular injury. Recently, Ebneter et al.[13] reported that resident microglia become activated and that blood-derived macrophages are recruited following RVO. Increased mononuclear phagocyte infiltration is a feature of several other retinal disease models including laser-induced choroidal neovascularization[25] and oxygen-induced retinopathy.[26] In these models, increased macrophage recruitment has been associated with more severe choroidal neovascularization and ischemic retinopathy, respectively. Currently, it is unknown whether blood-derived macrophages and activated microglia play distinct roles in RVO. In the future, it will be important to determine the roles of both of these cell types in the pathobiology of RVO.

Other groups have used mouse RVO as a model in which to study various aspects of retinal vascular disease. We find that RVO induces transient retinal edema, which agrees with findings from other groups.[13–15,17] Fuma and colleagues[14] induced vein occlusion in three vessels in several strains of

mouse and found variable susceptibility to RVO across strains. Interestingly, they did not find an RVO phenotype when the model was performed in C57BL/6J mice, which differs from our findings. This difference may be due to the fact that our mice were aged 7 to 9 months to more closely mirror the age of humans typically affected by RVO. By contrast, Fuma et al. used 7-week-old mice. Mouse age has been shown to have dramatic impacts on phenotype in other models of retinal disease,[27,28] and it will be important to further explore the impact of mouse age in the future. In other respects, our results are similar to those of Fuma et al.[14] in that we also find cystic intraretinal edema, which peaks early and gradually improves over 7 days. Fuma et al. had a higher incidence of retinal hemorrhage than we saw in our RVO cohort; however, this is likely due to the fact that they occluded multiple veins rather than a single vein, which would be expected to generate a more severe phenotype.

One limitation of our study is that we cannot differentiate local ocular effects of aldosterone from systemic effects of aldosterone treatment. The fact that we can detect changes in the localization of GFAP, AQP4, and Kir4.1 in aldosterone-treated mice prior to any other experimental manipulation demonstrates that aldosterone is mediating local effects prior to RVO. However, potential systemic effects of aldosterone treatment will require future study.

In conclusion, we have shown that mouse RVO leads to retinal edema and mild retinopathy manifest as occasional retinal hemorrhage. This phenotype is associated with mononuclear phagocyte recruitment and MG dysfunction. Low levels of systemic aldosterone exposure result in more severe and long-lasting edema as well as severe retinopathy following RVO. This suggests that aldosterone or the mineralocorticoid receptor may therefore be therapeutic targets in retinal vascular diseases including RVO, diabetes, retinopathy of prematurity, radiation retinopathy and others.

Acknowledgments

Disclosure: **M.J. Allingham**, None; **N. Tserentsoodol**, None; **P. Saloupis**, None; **P.S. Mettu**, None; **S.W. Cousins**, None

References

1. Campochiaro PA, Sophie R, Pearlman J, et al. Long-term outcomes in patients with retinal vein occlusion treated with ranibizumab: the RETAIN study. *Ophthalmology*. 2014;121:209–219.
2. Scott IU, VanVeldhuisen PC, Ip MS, et al. Effect of bevacizumab vs aflibercept on visual acuity among patients with macular edema due to central retinal vein occlusion. *JAMA*. 2017;317:2072.
3. Wykoff CC, Brown DM, Croft DE, Major JC, Wong TP. Progressive retinal nonperfusion in ischemic central retinal vein occlusion. *Retina*. 2015;35:43–47.
4. Keidar S, Hayek T, Kaplan M, et al. Effect of eplerenone, a selective aldosterone blocker, on blood pressure, serum and macrophage oxidative stress, and atherosclerosis in apolipoprotein E-deficient mice. *J Cardiovasc Pharmacol*. 2003;41:955–963.
5. Pruthi D, Mccurley A, Aronovitz M, Galayda C, Karumanchi SA, Jaffe IZ. Aldosterone promotes vascular remodeling by direct effects on smooth muscle cell mineralocorticoid receptors. *Arterioscler Thromb Vasc Biol*. 2014;34:355–364.
6. Pitt B, Zannad F, Remme WJ, et al. The effect of spironolactone on morbidity and mortality in patients with severe heart failure. Randomized Aldactone Evaluation Study Investigators. *N Engl J Med*. 1999;341:709–717.
7. Pitt B, Remme W, Zannad F, et al. Eplerenone, a selective aldosterone blocker, in patients with left ventricular dysfunction after myocardial infarction. *N Engl J Med*. 2003;348:1309–1321.
8. Zhao M, Valamanesh F, Celerier I, et al. The neuroretina is a novel mineralocorticoid target: aldosterone up-regulates ion and water channels in Müller glial cells. *FASEB J*. 2010;24:3405–3415.
9. Wilkinson-Berka JL, Tan G, Jaworski K, Miller AG. Identification of a retinal aldosterone system and the protective effects of mineralocorticoid receptor antagonism on retinal vascular pathology. *Circ Res*. 2009;104:124–133.
10. Allingham MJ, van Buul JD, Burridge K. ICAM-1-mediated, Src- and Pyk2-dependent vascular endothelial cadherin tyrosine phosphorylation is required for leukocyte transendothelial migration. *J Immunol*. 2007;179:4053–4064.
11. Rehak M, Hollborn M, Iandiev I, et al. Retinal gene expression and Müller cell responses after branch retinal vein occlusion in the rat. *Invest Ophthalmol Vis Sci*. 2009;50:2359–2367.
12. Rehak M, Drechsler F, Köferl P, et al. Effects of intravitreal triamcinolone acetonide on retinal gene expression in a rat model of central retinal vein occlusion. *Graefes Arch Clin Exp Ophthalmol*. 2011;249:1175–1183.
13. Ebneter A, Kokona D, Schneider N, Zinkernagel MS. Microglia activation and recruitment of circulating macrophages during ischemic experimental branch retinal vein occlusion. *Invest Ophthalmol Vis Sci*. 2017;58:944–953.
14. Fuma S, Nishinaka A, Inoue Y, et al. A pharmacological approach in newly established retinal vein occlusion model. *Sci Rep*. 2017;7:43509.
15. Dominguez E, Raoul W, Calippe B, et al. Experimental branch retinal vein occlusion induces upstream pericyte loss and vascular destabilization. *PLoS One*. 2015;10:e0132644.
16. Zhang H, Sonoda K-H, Qiao H, Oshima T, Hisatomi T, Ishibashi T. Development of a new mouse model of branch retinal vein occlusion and retinal neovascularization. *Jpn J Ophthalmol*. 2007;51:251–257.
17. Ebneter A, Agca C, Dysli C, Zinkernagel MS. Investigation of retinal morphology alterations using spectral domain optical coherence tomography in a mouse model of retinal branch and central retinal vein occlusion. *PLoS One*. 2015;10:e0119046.
18. Bodary PF, Sambaziotis C, Wickenheiser KJ, Rajagopalan S, Pitt B, Eitzman DT. Aldosterone promotes thrombosis formation after arterial injury in mice. *Arterioscler Thromb Vasc Biol*. 2006;26:233.
19. Liu S, Xie Z, Daugherty A, et al. Mineralocorticoid receptor agonists induce mouse aortic aneurysm formation and rupture in the presence of high salt. *Arterioscler Thromb Vasc Biol*. 2013;33:1568–1579.
20. Gaddam KK, Pimenta E, Husain S, Calhoun DA. Aldosterone and cardiovascular disease. *Curr Probl Cardiol*. 2009;34:51–84.
21. Reichenbach A, Wurm A, Pannicke T, Iandiev I, Wiedemann P, Bringmann A. Müller cells as players in retinal degeneration and edema. *Graefes Arch Clin Exp Ophthalmol*. 2007;245:627–636.
22. Nagelhus EA, Horio Y, Inanobe A, et al. Immunogold evidence suggests that coupling of K+ siphoning and water transport in rat retinal Müller cells is mediated by a coenrichment of Kir4.1 and AQP4 in specific membrane domains. *Glia*. 1999;26:47–54.
23. Tretiach M, Madigan MC, Wen L, Gillies MC. Effect of Müller cell co-culture on in vitro permeability of bovine retinal vascular endothelium in normoxic and hypoxic conditions. *Neurosci Lett*. 2005;378:160–165.
24. Yafai Y, Iandiev I, Lange J, et al. Müller glial cells inhibit proliferation of retinal endothelial cells via TGF-β2 and Smad signaling. *Glia*. 2014;62:1476–1485.
25. Caicedo A, Espinosa-Heidmann DG, Piña Y, Hernandez EP, Cousins SW. Blood-derived macrophages infiltrate the retina and activate Müller glial cells under experimental choroidal neovascularization. *Exp Eye Res*. 2005;81:38–47.

26. Deliyanti D, Miller AG, Tan G, Binger KJ, Samson AL, Wilkinson-Berka JL. Neovascularization is attenuated with aldosterone synthase inhibition in rats with retinopathy. *Hypertension*. 2012;59:607–613.

27. Espinosa-Heidmann DG, Suner I, Hernandez EP, Frazier WD, Csaky KG, Cousins SW. Age as an independent risk factor for severity of experimental choroidal neovascularization. *Invest Ophthalmol Vis Sci*. 2002;43:1567–1573.

28. Espinosa-Heidmann DG, Malek G, Mettu PS, et al. Bone marrow transplantation transfers age-related susceptibility to neovascular remodeling in murine laser-induced choroidal neovascularization. *Invest Ophthalmol Vis Sci*. 2013;54:7439–7449.

Investigative Ophthalmology & Visual Science